Chapter 6

Proposed Registration Procedure

The proposed registration procedure is explained in this chapter. This registration is seen as if it were done on a new subject from a statistical sample of skull geometries. To illustrate the procedure a generic skull shape is deformed into a representation of the orthognathic skull.

Although a completely automatic registration to such a complex shape would be ideal, a semi-automatic registration tool is described that requires very little user interference, apart from setting up the problem and describing constraints. In future work proposed on a sample of human skull geometries, the registration could be done in conjunction with an anthropologist or medical expert. In this way the correct features to use during registration should be kept and a new subject is registered with only the relevant features in mind.

In this example, the user of this registration tool could be expected to manipulate the target and generic geometries so that the influence of the sinuses for example is minimised or removed. This could be done by manually allocating areas of the geometry as unallowed. During registration, the displacements to fit unallowed parts of the surface is ignored and the generic surface is moved using only the registration with higher confidence. A flow chart of the registration procedure assembled from various methods discussed in this report is visible in Figure 6.1.

The registration is done on a generic tetrahedral mesh, generated from the generic surface using TetGen [9]. The generic representation then consists of the original surface and the volume mesh. The tetrahedral mesh is deformed using the registration of the surface mesh.

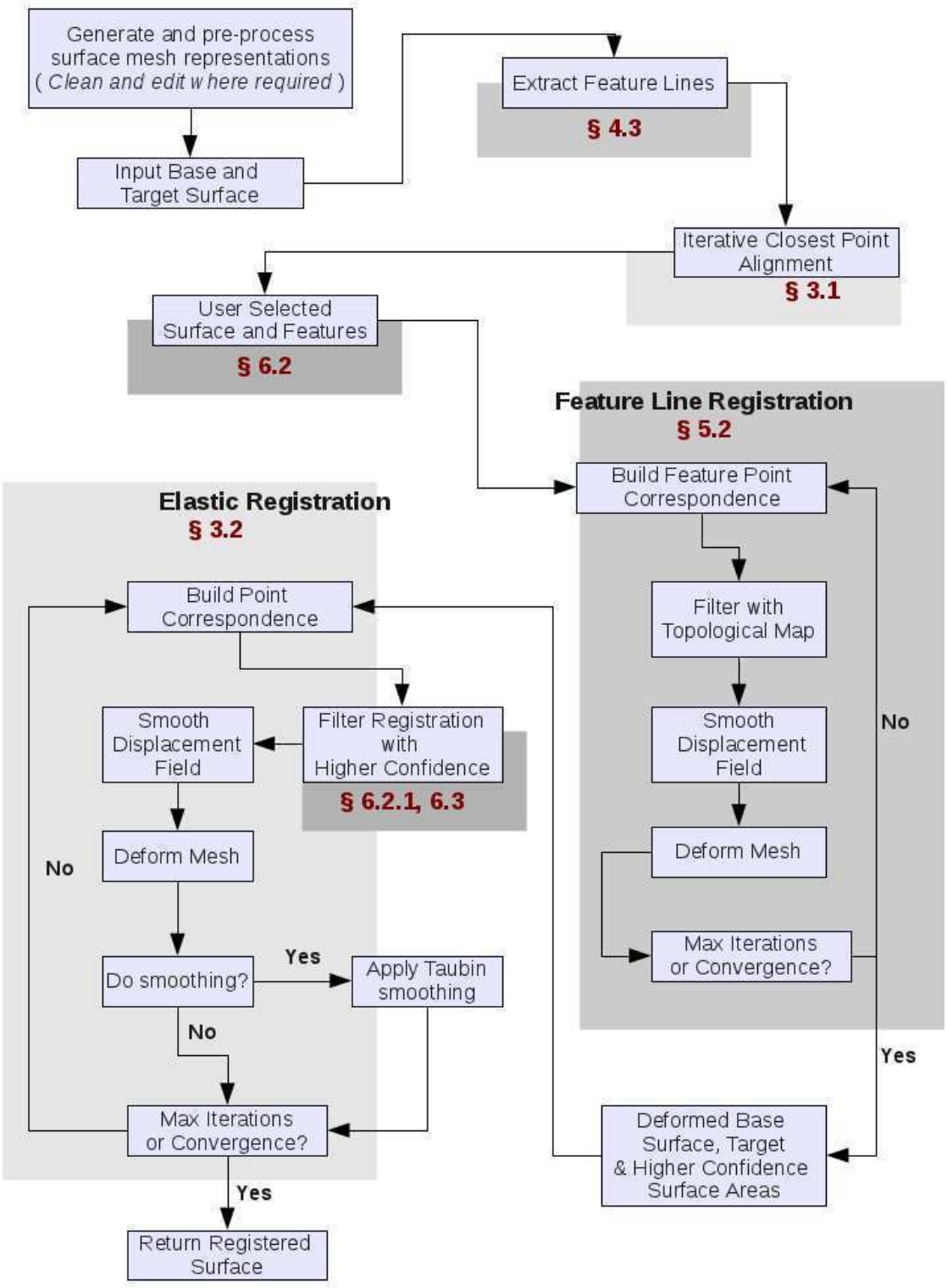

Figure 6.1: Flow diagram illustrating the various components of the registration procedure proposed and implemented.

UNIVERSITEIT VAN PRETORIA
UNIVERSITY OF PRETORIA
YUNIBESITHI YA PRETORIA

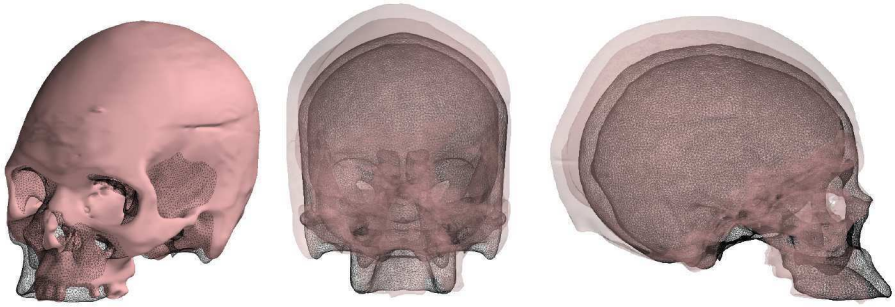

(a) (b) (c)

Figure 6.2: (a) Original position of the orthognathic skull geometry relative to the smoothed base skull. (b) Frontal and (c) lateral view of the orthognathic skull and base skull represented by the black wire-frame mesh.

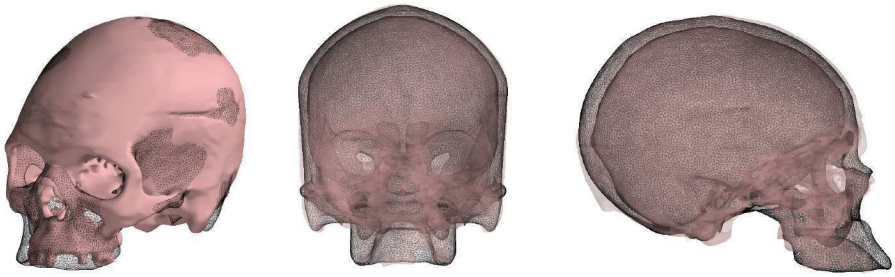

(a) (b) (c)

Figure 6.3: (a) Rigid registration position of the orthognathic skull geometry relative to the smoothed base skull after an isotropic ICP registration. (b) Frontal and (c) lateral view of the orthognathic skull and base skull represented by the black wire-frame mesh.

6.1 Step 1: Rotate, Scale and Translate

Before deforming the generic skull shape into a representation of the orthognathic skull form, a rigid registration is performed. Using the implemented ICP procedure, the orthognathic skull is registered and aligned to the generic shape. The orthognathic skull in it's original position relative to the symmetric base mesh is visible in Figure 6.2. The result after performing an isotropic scale ICP is visible in Figure 6.3.

UNIVERSITEIT VAN PRETORIA
UNIVERSITY OF PRETORIA
YUNIBESITHI YA PRETORIA

6.2 Step 2: Use Lines of Curvature

After a rigid registration to scale and align the target geometry to the generic mesh, a feature line registration is performed. As an example, only user selected features on the generic mesh is kept during the registration. The reason for doing this in the example is the vast difference in internal features between the skull geometries as visible in the facial regions as depicted in Figures 2.6 and 2.7.

The broken and decayed areas in the skull are also extracted as features and could be registered to different areas in other skull geometries. The generic mesh is created from an edited and smoothed version of the prognathic skull surface mesh. In removing areas of the decayed skull, most of the features internal to the facial region on the generic skull form are artificial. Mainly features with greater confidence are therefore selected on the generic skull shape and allowed to register. The surface in this edited area is selected manually. These areas are allowed to register but shouldn't be registered by the target.

The sinuses also have vastly different shapes, as visible in Figure 2.5. These along with other internal features of the facial area are removed from the allowable feature lines and surfaces on the generic skull shape for this example.

The user selected allowable features for registration in this example are displayed on the generic skull shape in Figure 6.4. In the proposed work on a sample of skulls however, the valid feature lines that would be found on all skull geometries would be allowed to register. These would be extracted from a fixed generic mesh and chosen as valid features with the help of a medical professional.

Registration of the allowable feature lines on the generic skull to the orthognathic form is displayed in Figure 6.5. In this figure, the generic features are first displayed in their original position on the top with the location of the deformed lines after registration to the orthognathic form below. For visual clarity, the feature lines extracted from the orthognathic skull is omitted.

User specified feature lines are again displayed in their deformed positions in Figure 6.6, along with the corresponding features on the target geometry. The unregistered features on the target are discarded and are not visible in this figure.

6.2.1 Feature Surfaces

The feature surfaces associated with the unregistered feature lines are extracted and classified as untrusted registration surfaces. This is done because registration

UNIVERSITEIT VAN PRETORIA
UNIVERSITY OF PRETORIA
YUNIBESITHI YA PRETORIA

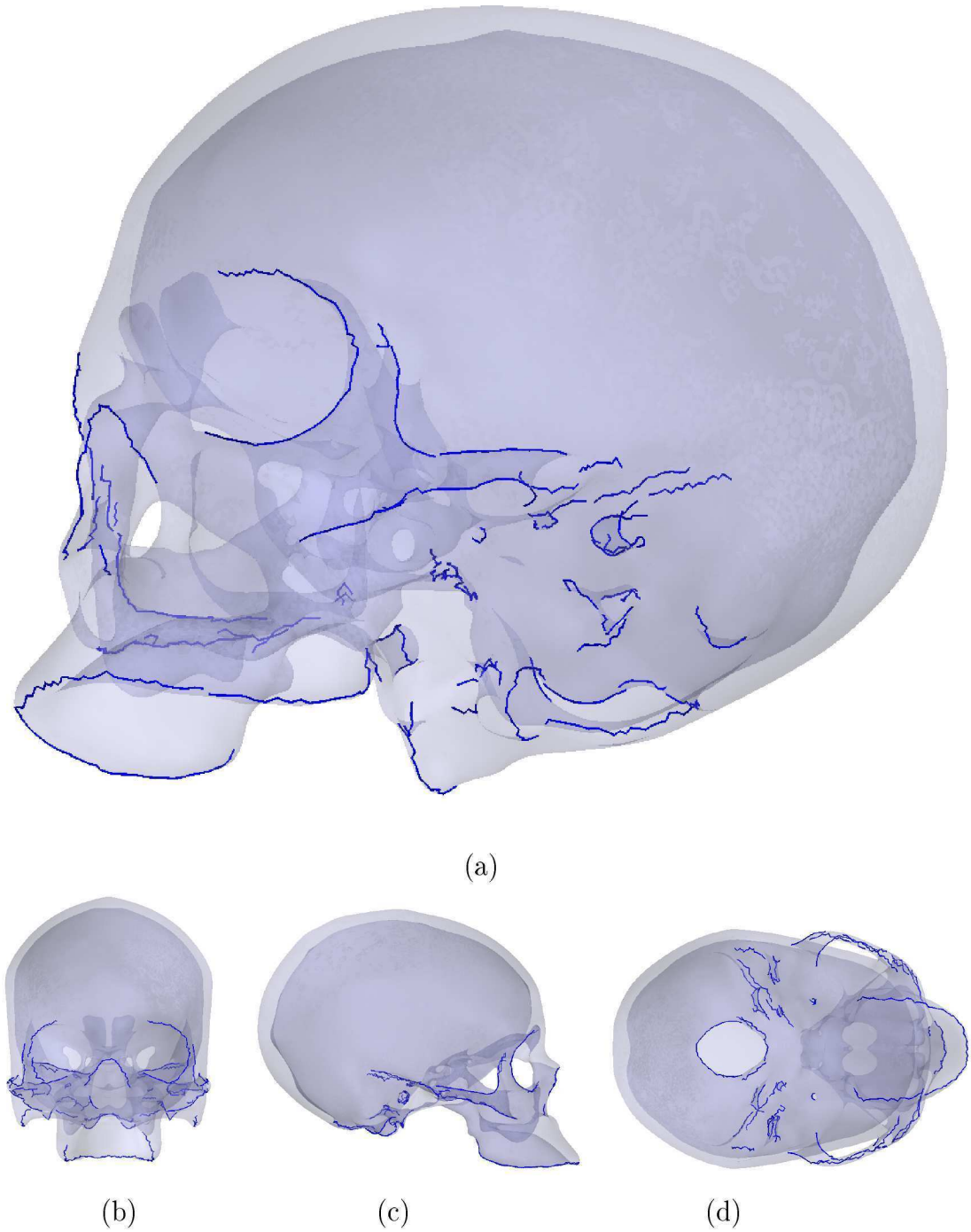

(a)

(b) (c) (d)

Figure 6.4: (a) User selected allowable features on the symmetric base skull geometry. (b) Frontal, (c) lateral and (d) lower view.

UNIVERSITEIT VAN PRETORIA
UNIVERSITY OF PRETORIA
YUNIBESITHI YA PRETORIA

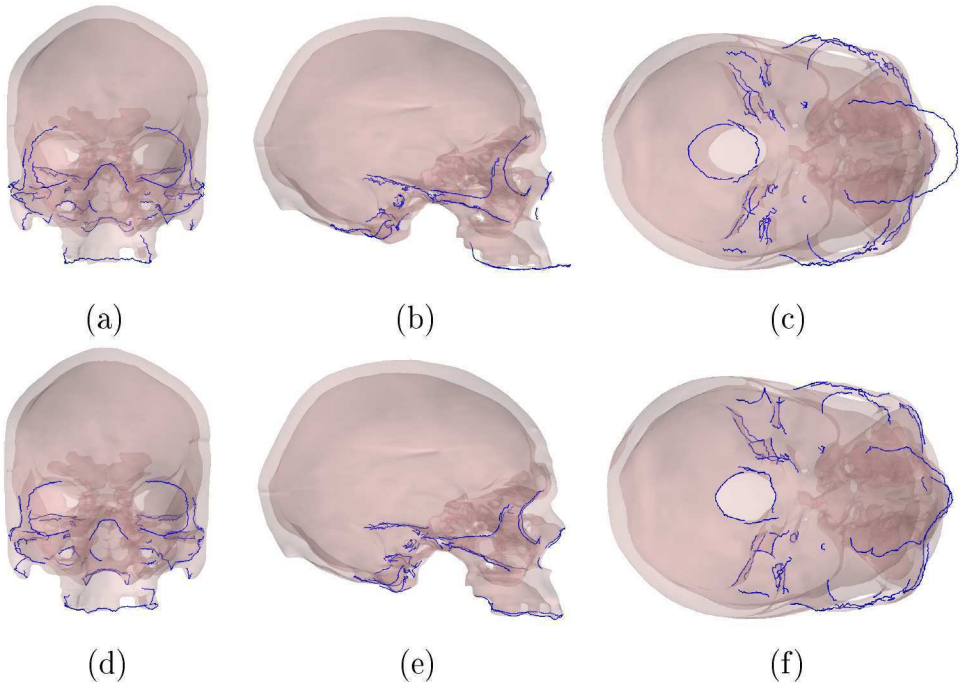

(a) (b) (c)

(d) (e) (f)

Figure 6.5: Registration of allowable base geometry features to the orthognathic skull. (a) Frontal, (b) lateral and (c) lower view of the base geometry features relative to the orthognathic skull. (d) Frontal, (e) lateral and (f) lower view of the base geometry features registered and deformed to the corresponding features on the orthognathic skull.

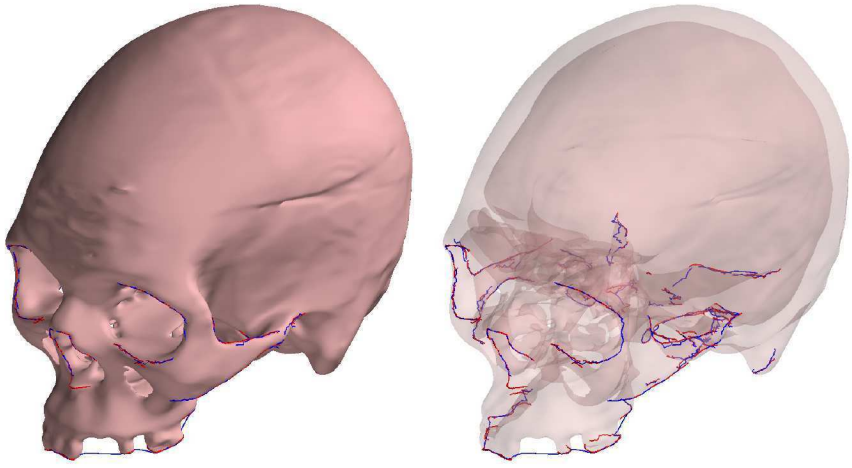

(a) (b)

Figure 6.6: Registration of allowable base geometry features to the orthognathic skull. (a) The registration result on an opaque target skull and (b) semi-transparent target surface. Blue lines indicate the features of the deformable surface with red lines indicating the target features.

UNIVERSITEIT VAN PRETORIA
UNIVERSITY OF PRETORIA
YUNIBESITHI YA PRETORIA

to unmatched features could result in a distorted mesh, as seen in Figures 5.14 through 5.16.

The feature points used in this example are classified using the result of the MLS method. Curvature information obtained on the geometries is used to construct feature lines. Using the magnitudes of the principal curvatures, the feature rich areas are described. All the feature points satisfying the chosen conditions on the generic and target mesh are illustrated in Figures 6.7 and 6.8. The values of 0.2 and 0.18 are arbitrarily chosen on the different skull geometries. This is done so that the same approximate size of the relative feature areas are highlighted. The curvature estimation was done before performing the scaling visible in Figures 6.2 and 6.3, so the difference is highly likely due to the difference in scale between the geometries at the time of curvature information extraction.

Using the user specified features on the base mesh and the registered feature lines on the target, the corresponding allowable feature points are chosen. The allowable feature points are displayed in Figures 6.9 and 6.10.

Allowable feature points are extracted using the following procedure on a given surface mesh:

- A $k-d$ tree representation of all the points in the extracted and thresholded set of feature lines is set up for nearest neighbour search.
- For each point within the set of feature points:
  - The closest point on a feature line is searched using the $k-d$ tree.
  - If the point closest to the feature point is on a user specified or registered line, the current point is added to a list of allowable feature points. If not, the current point is added to a list of low confidence feature points.

The allowable and low confidence feature points for both the base and target mesh are extracted. The list of triangles representing each surface is inspected. A list of low confidence triangles is set up using the allowable and low confidence feature points.

A triangle is marked as a low confidence surface triangle if any one of it's nodes are in the list of low confidence feature points. Registration is then only allowed to the surface triangles and points with higher confidence.

UNIVERSITEIT VAN PRETORIA
UNIVERSITY OF PRETORIA
YUNIBESITHI YA PRETORIA

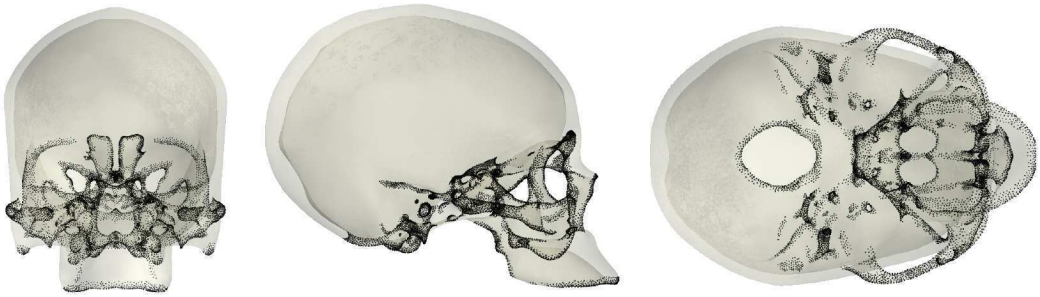

(a) (b) (c)

Figure 6.7: All feature points on the symmetric base skull for $\kappa_{\max} > 0.2$ and $\kappa_{\min} < -0.2$. (a) Frontal, (b) lateral and (c) lower view.

(a) (b) (c)

Figure 6.8: All feature points on the orthognathic target skull for $\kappa_{\max} > 0.18$ and $\kappa_{\min} < -0.18$. (a) Frontal, (b) lateral and (c) lower view.

(a) (b) (c)

Figure 6.9: Feature points on the symmetric base skull for $\kappa_{\max} > 0.2$ and $\kappa_{\min} < -0.2$ corresponding to the user specified allowable feature lines in Figure 6.4. (a) Frontal, (b) lateral and (c) lower view.

UNIVERSITEIT VAN PRETORIA
UNIVERSITY OF PRETORIA
YUNIBESITHI YA PRETORIA

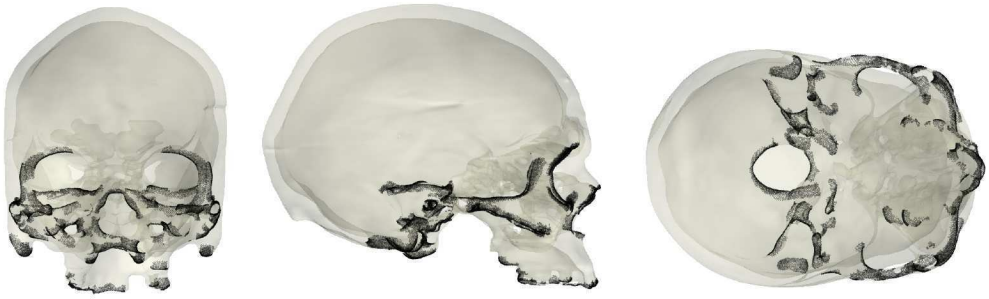

(a) (b) (c)

Figure 6.10: Feature points on the orthognathic target skull for $\kappa_{\max} > 0.18$ and $\kappa_{\min} < -0.18$ corresponding to the user specified allowable feature lines in Figure 6.6. (a) Frontal, (b) lateral and (c) lower view.

6.3 Step 3: Register Allowable Surface

The tetrahedral mesh is deformed using the Gaussian weighting function implemented into the registration procedure. Deformation during feature line registration is still performed in the same way using the registered position of points in the set of feature lines. To make the elastic surface registration more robust to unwanted deformation and the possible inversion of elements, the deformation obtained as a result of the Gaussian function is smoothed again using Taubin smoothing.

Modifications to the original registration procedure is outlined in this subsection. The model shape $\mathcal{M}$ not only consists of triangles but also tetrahedral elements. Key steps to deform the generic shape $\mathcal{M}$ into the target $\mathcal{P}$ with the modified version of the elastic registration procedure are:

- The deformed generic tetrahedral shape after feature line registration is used as the initial condition before elastic surface registration.
- Registered positions are only found for higher confidence points on both the generic and target surfaces. These allowable points can be user specified or obtained after the feature line registration procedure as described in subsection 6.2.1.
- Registration to any part of the surface (either points or surfaces) with a low confidence level is ignored.
- Only the registration of surface points with a higher confidence level is used to deform the tetrahedral mesh. An initial update on tetrahedral mesh

UNIVERSITEIT VAN PRETORIA
UNIVERSITY OF PRETORIA
YUNIBESITHI YA PRETORIA

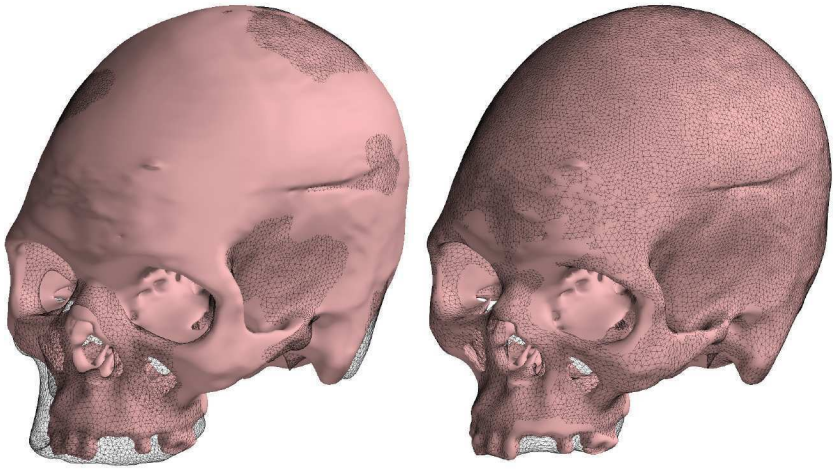

(a) (b)

Figure 6.11: Elastic registration on the orthognathic skull. (a) The rigid registration result to align the orthognathic skull to the deformable mesh with (b) the registration result at iteration 60. This registration result is obtained after an initial allowable feature registration and filtering for allowable surfaces. The compared result of Figure 5.14 employed full feature and subsequent full elastic surface registration.

nodal coordinates are obtained with higher confidence registrations and Equation (3.8).

- Taubin smoothing is applied to the computed deformation field.
- After the deformation field is smoothed, it is applied to the generic tetrahedral mesh. Inverted elements would restrict the use of the mesh post-registration. The reason for smoothing the deformation is to make the deformed mesh more resilient to unwanted distortion. Unfortunately a simple smoothing strategy does not penalise unwanted distortion precisely and element inversion could still occur.

The result of performing an elastic registration on the orthognathic skull with user specified and automatic constraints is visible in Figures 6.11 through 6.13. For this example, an allowable surface for registration on the generic skull is done manually. Also, the internal surface of the facial area is selected manually, and registration to this part of the generic mesh is not allowed.

Higher confidence nodes on the generic surface and orthognathic surface is obtained after feature line registration as described in section 6.2. Registration is then

UNIVERSITEIT VAN PRETORIA
UNIVERSITY OF PRETORIA
YUNIBESITHI YA PRETORIA

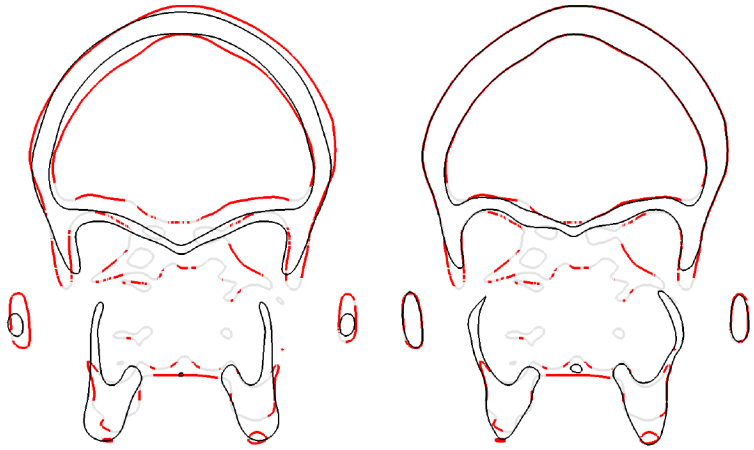

(a) (b)

Figure 6.12: Frontal view of elastic registration on the orthognathic skull for automatically selected allowable features. (a) The target and deformable geometry after isotropic scale ICP registration. After the initial registration of selected features in Figure 6.6, elastic surface registration is performed and smoothed resulting in (b) the smoothed registration result at iteration 60. The gray and red line sections represent the target surface. Grey represents the automatically discarded areas while the red lines represent the allowable and featureless target surface in the same plane as Figure 5.15. The black line represents the deformable mesh surface.

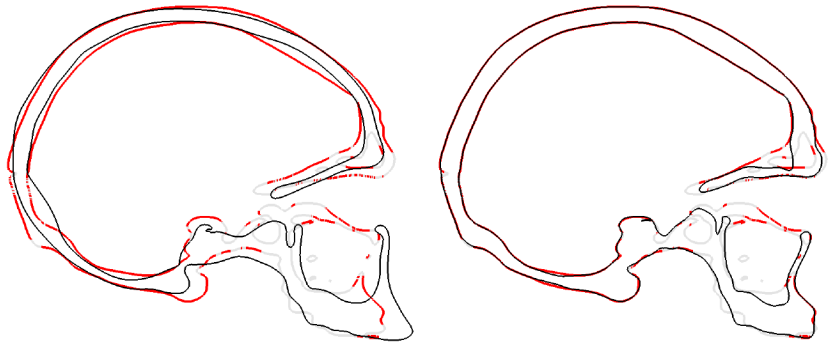

(a) (b)

Figure 6.13: Lateral view of elastic registration on the orthognathic skull for automatically selected allowable features. (a) The target and deformable geometry after isotropic scale ICP registration. After the initial registration of selected features in Figure 6.6, elastic surface registration is performed and smoothed resulting in (b) the registration result at iteration 60. The gray and red line sections represent the target surface. Grey represents the automatically discarded areas while the red lines represent the allowable and featureless target surface in the same plane as Figure 5.16. The black line represents the deformable mesh surface.

UNIVERSITEIT VAN PRETORIA
UNIVERSITY OF PRETORIA
YUNIBESITHI YA PRETORIA

done using the higher confidence surface triangles on the orthognathic skull and the user selected allowable surface triangles on the generic skull.

Comparing the cut planes in Figures 6.12 and 6.13 to those in Figures 5.15, 5.16 and 5.17, there is a possible improvement on the result at iteration 60 if registration is approached in this selective manner. In doing a proper registration, additional user interference may still be required to obtain a better representation of the target skull geometry in this example. Although this is not ideal, at least the amount of user interference in performing an elastic registration on these complex geometries is reduced.

The target geometry in this example is left totally unedited with all the user specified constraints and restrictions applied to only the generic deformable mesh. Compared to the original full elastic registration, this combined procedure implemented translates to far less user input needed in registering a large statistical sample of skull geometries. This is because each new geometry could be used with very little pre-registration editing required. It is however noticed in the cut planes of Figures 6.12 and 6.13 that editing a target geometry before registration could result in an improved representation of that skull.

As a further example of registration with the proposed method using user specified and automatic constraints, both prognathic and orthognathic skull geometries are registered. The target shapes are the original surfaces visible in Figure 6.14 (a) and (d). The procedure for matching feature lines and determining lower confidence registrations is then applied to both models and the generic surface is deformed into the target representations visible in Figure 6.14 (b) and (e).

If the generic model is deformed into a target shape and then the reflected target shape, the average of the two deformed meshes can be used to create a symmetric version of the target. Examples of the approximate symmetric versions of both the orthognathic and prognathic skull geometry are illustrated in Figures 6.14 (c) and (f).

6.4 Step 5: Mesh Quality

Mesh quality can be improved by using the quality improvement toolbox MESQUITE [5]. In this example, a tetrahedral finite element mesh is generated on the average symmetric skull surface. This average symmetric skull surface is determined after first creating symmetric versions of the two geometries as illustrated in Fig-

UNIVERSITEIT VAN PRETORIA
UNIVERSITY OF PRETORIA
YUNIBESITHI YA PRETORIA

Figure 6.14: (a) Orthognathic target skull geometry with (b) the registration result and (c) the symmetric version on the registration result. (d) Prognathic target skull geometry with (e) the registration result and (f) the symmetric version on the registration result.

UNIVERSITEIT VAN PRETORIA
UNIVERSITY OF PRETORIA
YUNIBESITHI YA PRETORIA

ures 6.14 (c) and (f). The tetrahedral mesh was generated using TetGen [9] and had 1′687′795 elements.

The mesh generated on the average skull surface was then deformed by doing an FEA where the target boundary positions is known and so a known displacement is applied to boundary nodes. This is done in the hope that the movement of internal nodes would occur in a reliable manner when deforming the average mesh back into prognathic and orthognathic representations.

Element inversion occurred for applied nodal displacement higher than approximately 40% of the actual displacement required when using simple linear elastic elements in the analysis. This is considered a problem because FEBio solves the large set of equations in a matrix free manner. The problem moves internal nodal coordinates using a linear elastic analysis and hits a wall if displacement updates cause element inversion.

It is decided to do a simple nodal coordinate update based on the displacement information up to the 40% mark. Mesh untangling and quality improvement is planned at the final stage. The displacement of the internal nodes with 40% of the boundary displacement applied is multiplied with a factor of 2.5. This displacement is then applied to the original internal nodal coordinates along with 100% known boundary displacement to create the mesh representing the prognathic and orthognathic skull.

6.4.1 Quality Metric

The quality metric used in this report is one of the tetrahedron shape measures used by Escobar *et al.* in constructing objective functions for mesh untangling and smoothing [29]. This quality metric is obtained by algebraic operation and can therefore be computed efficiently.

The chosen quality metric can be constructed as in the work done by Escobar *et al.* [29]. If $\mathcal{T}$ is a tetrahedral element in the physical space whose vertices are given by $\mathbf{x}_j = \begin{pmatrix} x_j & y_j & z_j \end{pmatrix}$, $j = 0, 1, 2, 3$ and $\mathcal{T}_R$ is the reference tetrahedron with vertices $\mathbf{u}_0 = \begin{pmatrix} 0 & 0 & 0 \end{pmatrix}$, $\mathbf{u}_1 = \begin{pmatrix} 1 & 0 & 0 \end{pmatrix}$, $\mathbf{u}_2 = \begin{pmatrix} 0 & 1 & 0 \end{pmatrix}$ and $\mathbf{u}_3 = \begin{pmatrix} 0 & 0 & 1 \end{pmatrix}$, a translation vector $\mathbf{x}_0$ can be chosen so that the affine map $\mathbf{x} = \mathbf{J}\mathbf{u} + \mathbf{x_0}$ takes $\mathcal{T}_R$ to $\mathcal{T}$. In this affine map, $\mathbf{J}$ represents the Jacobian matrix

UNIVERSITEIT VAN PRETORIA
UNIVERSITY OF PRETORIA
YUNIBESITHI YA PRETORIA

referenced to node $\mathbf{x}_0$ and can be determined from

$$\mathbf{J} = \begin{bmatrix} x_1 - x_0 & x_2 - x_0 & x_3 - x_0 \\ y_1 - y_0 & y_2 - y_0 & y_3 - y_0 \\ z_1 - z_0 & z_2 - z_0 & z_3 - z_0 \end{bmatrix}. \tag{6.1}$$

A tetrahedron $\mathcal{T}_I$ is equilateral with all of its edges length one. The vertices of $\mathcal{T}_I$ are located at $\mathbf{v}_0 = \begin{pmatrix} 0 & 0 & 0 \end{pmatrix}$,$\mathbf{v}_1 = \begin{pmatrix} 1 & 0 & 0 \end{pmatrix}$,$\mathbf{v}_2 = \begin{pmatrix} 1/2 & \sqrt{3}/2 & 0 \end{pmatrix}$ and $\mathbf{v}_3 = \begin{pmatrix} 1/2 & \sqrt{3}/6 & \sqrt{2}/\sqrt{3} \end{pmatrix}$. If $\mathbf{v} = \mathbf{W}\mathbf{u}$ is a linear map that takes $\mathcal{T}_R$ to $\mathcal{T}_I$, the Jacobian matrix is given by

$$W = \begin{bmatrix} 1 & 1/2 & 1/2 \\ 0 & \sqrt{3}/2 & \sqrt{3}/6 \\ 0 & 0 & \sqrt{2}/\sqrt{3} \end{bmatrix}. \tag{6.2}$$

The affine map that now takes $\mathcal{T}_I$ to $\mathcal{T}$ is given by $\mathbf{x} = \mathbf{J}\mathbf{W}^{-1}\mathbf{v} + \mathbf{x_0}$, and its Jacobian matrix is $\mathbf{Q} = \mathbf{J}\mathbf{W}^{-1}$. The matrix norms, determinant or trace of $\mathbf{Q}$ can be used to construct algebraic quality measures of $\mathcal{T}$. The quality metric chosen and reported in Table 6.1 is determined for the m^{th} tetrahedron as [29]:

$$q_m = \frac{3\sigma_m^{2/3}}{|\mathbf{Q}_m|^2}, \tag{6.3}$$

where $\sigma = \det(\mathbf{Q})$ and $|\mathbf{Q}|$ is the Frobenius norm of the Jacobian matrix $\mathbf{Q}$ defined by $|\mathbf{Q}| = \sqrt{\text{tr}\,(\mathbf{Q}^T\mathbf{Q})}$. This quality metric is slightly modified by Escobar *et al.* [29] by introducing the use of the positive and increasing function $h\,(\sigma)$ instead of the original σ. The quality metric is then rewritten as:

$$q_m = \frac{3h\,(\sigma_m)^{2/3}}{|\mathbf{Q}_m|^2}. \tag{6.4}$$

This ensures element quality to be in the range of $(0, 1]$. The reason for doing this is twofold.

- An inverted element has a negative Jacobian and so determining $\det(\mathbf{Q})^{2/3}$ poses a problem. The positive and increasing function $h(\sigma)$ actually allows the calculation of element quality for a negative determinant of the Jacobian matrix.

UNIVERSITEIT VAN PRETORIA
UNIVERSITY OF PRETORIA
YUNIBESITHI YA PRETORIA

- The inverted elements have a quality close to zero so that the inverse of the element quality approaches infinity as elements become more degenerate. The inverse of the modified quality metric is set to a range $[1, \infty)$ using this modification. The inverted metric is used to construct an objective function for simultaneous mesh untangling and smoothing during an optimisation procedure by Escobar *et al.* [29]. In constructing the objective function per element in this manner, inversion or degeneration of tetrahedral elements is penalised heavily.

The positive and increasing function used is defined by [29]

$$h(\sigma) = \frac{1}{2}\left(\sigma + \sqrt{\sigma^2 + 4\delta^2}\right). \tag{6.5}$$

Here δ is chosen and applied when determining the quality of all elements in such a way that

$$\delta \geq \delta_{\min} = \begin{cases} \sqrt{\zeta\left(\zeta - \sigma_{\min}\right)} & \text{if } \sigma_{\min} < \zeta \\ 0 & \text{if } \sigma_{\min} \geq \zeta \end{cases} \tag{6.6}$$

where ζ is taken as approximately machine epsilon ($0 < \zeta \ll 1$) or some user selected minimum. This means that the final element quality for all elements can only be determined after inspecting all elements for inversion. Constructing ζ in this way insures $h(\sigma) \geq \zeta$. The implementation done for this report used python code with $\zeta = 10^{-8}$.

6.4.2 Usable Skull Mesh Generation

The meshes used as an example to again analyse and determine difference in stress field due to cranial shape variation in masticatory induced stress is first generated on the average skull mesh surface. This mesh generated consists of 1′687′795 tetrahedral elements with a minimum element quality of 0.155 and an average quality of 0.797, using the quality metric in Equation (6.4).

The tetrahedral mesh is deformed into the symmetric prognathic and orthognathic skull representations. These representations are obtained by applying the registration procedure discussed in this chapter. To obtain a prognathic and orthognathic representation of the tetrahedral mesh generated on the average surface, the following is done:

UNIVERSITEIT VAN PRETORIA
UNIVERSITY OF PRETORIA
YUNIBESITHI YA PRETORIA

	Original	Prognathic		Orthognathic	
		Initial	Improved	Initial	Improved
$\sigma < 0$	0	10	0	15	4
δ	0	0.0001169	0	0.0003271	0.0002487
min (q)	0.1549	8.48e-6	0.1042	7.48e-6	8.5e-6
max (q)	0.99998	0.99971	0.99966	0.99984	0.99958
average (q)	0.79713	0.78306	0.80434	0.78734	0.80894
$q < 0.5$	81568	90603	33173	87702	30886
$q < 0.15$	0	26	2	21	4

Table 6.1: Mesh Quality compared to original mesh generated from the symmetric skull surface. The tetrahedral mesh representations representing the prognathic and orthognathic skull shapes are then improved using MESQUITE [5] with boundary nodes constrained.

- 40% of the known nodal displacement to either the prognathic or orthognathic representation is applied to the boundary nodes of the tetrahedral mesh. This is used in a linear elastic finite element analysis with $E = 16$ GPa and $\nu = 0.3$, the same material properties used in the initial analysis to represent a linear elastic bone material. The displacement is known as all of the surface mesh representations have one-to-one correspondence and identical topology.

- Nodal displacement is extrapolated to the 100% mark. The updated nodal coordinates after performing an FEA is used and the displacement from the initial undeformed configuration to the deformed configuration is applied to the original tetrahedral mesh using a scale factor of 2.5. Linear elastic elements are used and so linear deformation may be assumed.

- The tetrahedral skull representation is optimised using the coordinates of internal nodes as design variables while the boundary surface nodes are constrained. The MESQUITE Mesh Quality Improvement Toolkit [5] is used in this step.

Original and improved mesh quality are visible in Table 6.1. Not only is the average quality of the mesh improved but the mesh is also untangled with the only inverted elements left after optimisation those on the surface where nodal coordinates are constrained. The four surface elements that remain inverted after quality improvement on the orthognathic skull mesh are shown in Figure 6.15.

These inverted elements are situated on the surface and is far removed from the

UNIVERSITEIT VAN PRETORIA
UNIVERSITY OF PRETORIA
YUNIBESITHI YA PRETORIA

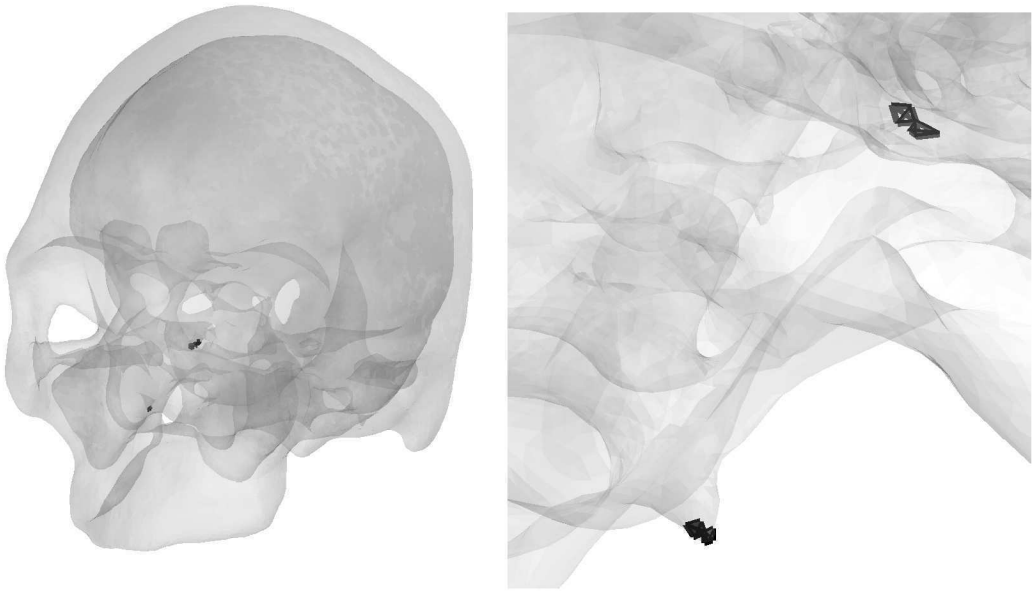

(a) (b)

Figure 6.15: Inverted elements retained after mesh improvement in the orthognathic skull representation. (a) Global position of inverted elements. (b) Detail showing the four inverted surface elements.

(a) (b) (c)

Figure 6.16: Mesh quality evaluated using Equation (6.4). (a) Symmetric prognathic skull representation. (b) Original mesh generated on the average surface using TetGen [9]. (c) Symmetric orthognathic skull representation.

UNIVERSITEIT VAN PRETORIA
UNIVERSITY OF PRETORIA
YUNIBESITHI YA PRETORIA

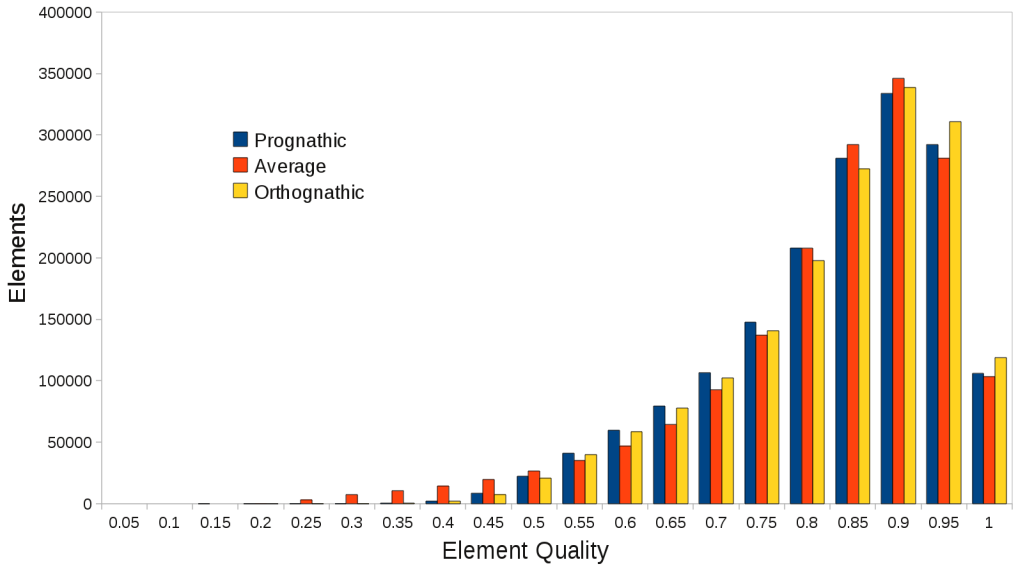

Figure 6.17: Histogram illustrating the element quality of the optimised prognathic and orthognathic mesh representations as well as the element quality of the original mesh generated on the average skull surface.

facial area of interest. It is therefore decided that the result obtained from an FEA would not suffer in their absence. These four elements are removed from all mesh representations so there could still remain an identical mesh topology for all meshes of interest. The final tetrahedral meshes representing the prognathic, orthognathic and average skull geometry are visible in Figure 6.16. All have identical mesh topology with a total of 1′687′791 elements. The histograms visible in Figure 6.17 show the distribution of element quality for all three of the meshes visible in Figure 6.16.

The mesh quality of these tetrahedral mesh skull representations are fairly consistent and would seem to be as a result of mainly the quality of the original mesh generated.

6.5 Analysis on Registered Skull Geometries

The three tetrahedral meshes illustrated in Figure 6.16 are analysed for molar bite force as an example. This is done to illustrate the benefit of having the same mesh topology with only a difference in nodal coordinates to represent all the geometries of interest.

The nodes where boundary conditions are applied in an FEA are the exact

UNIVERSITEIT VAN PRETORIA
UNIVERSITY OF PRETORIA
YUNIBESITHI YA PRETORIA

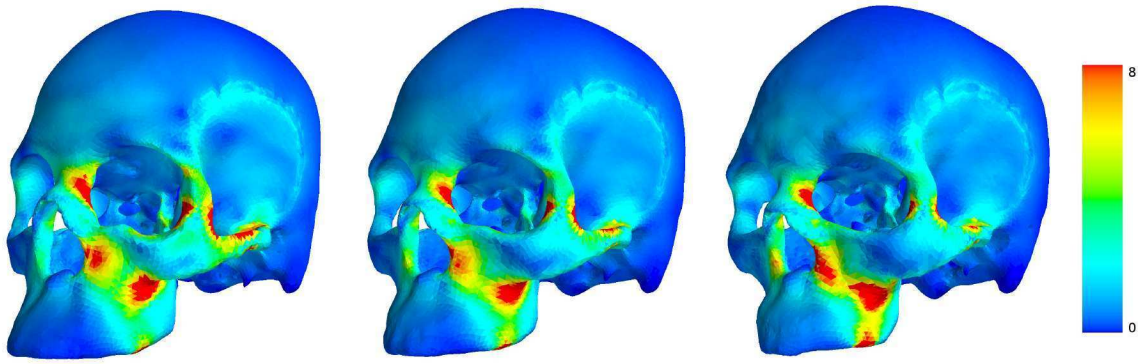

(a) (b) (c)

Figure 6.18: Von Mises stress contours for a molar bite scaled to show a maximum of 8 MPa. (a) Prognathic, (b) Average and (c) Orthognathic skull shape.

same nodes in this case for all three meshes. Boundary conditions are set up as in section A.4 of Appendix A where the initial finite element analysis on the skull shapes is discussed. The direction of the forces for the average case is obtained by interpolating between the known directions in the prognathic and orthognathic case. Material properties are selected as that of the linear elastic material also used in the initial analysis with Young's modulus $E = 16$ GPa and Poisson's ratio $\nu = 0.3$.

The results of the FEA can be manipulated in a few ways if one-to-one mesh correspondence is available for all the geometries analysed. In Figure 6.18, the Von Mises stresses are given in the usual way with all stresses higher than 8 MPa simply shown in red. The maximum Von Mises stress for this analysis is 18.56 MPa for the prognathic skull form, 15.334 MPa on the average and 17.589 MPa for the orthognathic skull form. These stresses fall into the same range and no artificial stress concentrations are present that do not occur in all three skull forms. The relative scale of the skull geometries allow comparison of the stress field without further manipulation or scaling.

In Figure 6.19, the resulting stress in the prognathic and orthognathic form are compared in a way that is possible due to one to one correspondence between all the meshes. Here the Von Mises stresses in the orthognathic skull form is subtracted from the prognathic skull form in an element-wise manner. This is done and illustrated on the mesh representing the average skull in Figure 6.19 (c).

Inter-patient variation in masticatory induced stress field is presented in Figure 6.19. It would appear from this analysis that there is a higher stress in the

UNIVERSITEIT VAN PRETORIA
UNIVERSITY OF PRETORIA
YUNIBESITHI YA PRETORIA

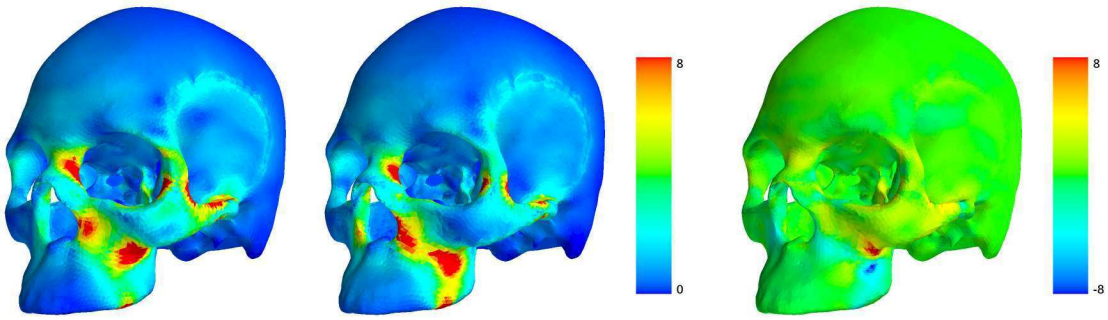

(a) (b) (c)

Figure 6.19: (a) The Von Mises stress in the prognathic skull shape plotted on the mesh representing the average shape. (b) The Von Mises stress in the orthognathic skull shape plotted on the mesh representing the average shape. (c) The difference in Von Mises stress between the prognathic and orthognathic finite element results $\sigma^{\text{vM}}_{\text{prognathic}} - \sigma^{\text{vM}}_{\text{orthognathic}}$ shown for the range $[-8, 8]$ MPa. All of the contours are plotted on the mesh representing the average skull shape. (a)-(b)=(c)

zygomatic arch and bridge of the nose in the prognathic skull form while the orthognathic form has a higher stress concentration in the maxilla or upper mandible. The locality of high variation in stress field is visible. Only the analysis on the masticatory induced stress during a molar bite is used as an example.

Conclusions on the link between prognathism and stress can be drawn from an analysis on more skulls as well as better detailed models. These conclusions should be done with the aid of an expert in the field such as an Anthropologist and is not done in this report.

6.5.1 The effect of non-unique registration on FEA result

The structural analysis (FEA) should ideally be done with a registration tool that produces unique and reliable representations and it is therefore proposed that the current procedure be improved further. It would be undesirable to assign significance to a specific variation in stress or some other quantity due to variation introduced by the elastic registration procedure.

Various meshes representing both the prognathic and orthognathic skull geometries are created in an attempt to quantify the effect of non-unique registration and discretisation on the FEA result. This is done following the same logic used to illustrate the sensitivity of the registration procedure to user selected smoothing parameters. The various meshes obtained for the femur geometry is visible in Fig-

UNIVERSITEIT VAN PRETORIA
UNIVERSITY OF PRETORIA
YUNIBESITHI YA PRETORIA

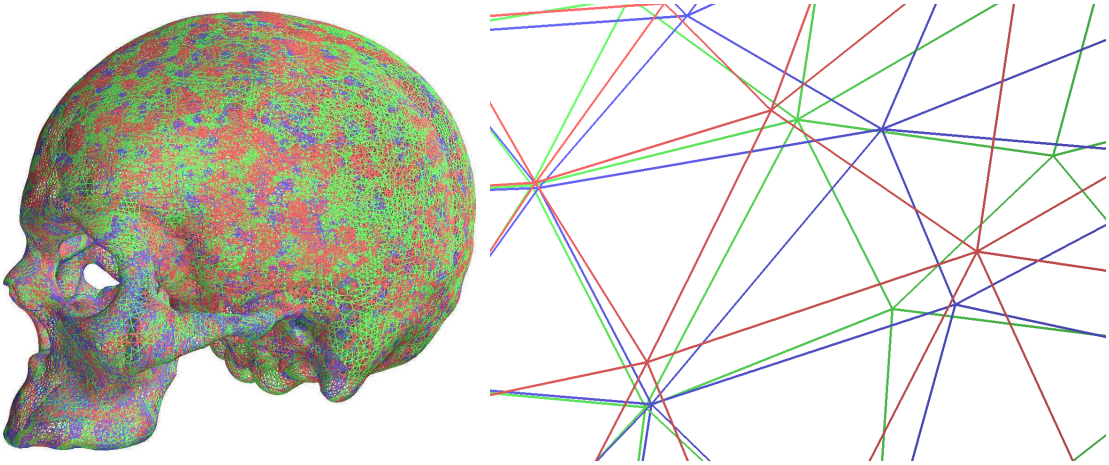

(a) (b)

Figure 6.20: (a) Three different meshes representing the orthognathic skull shape. (b) Detail of the meshes in (a) illustrating a difference in nodal coordinate positions. This is done for both prognathic and orthognathic skull shape. Three meshes representing each shape is used to quantify the influence the uniqueness of a registration result obtained by this method has on the final FEA result.

ure 3.8. An FEA on all the meshes could produce an approximate quantification of the uncertainty in the results displayed in Figure 6.19 (c).

The surface representing the symmetric version of the orthognathic skull in Figure 6.14 (c) is used as the target surface during a registration procedure. Two elastic surface registrations are performed with the generic mesh used in this chapter. The smoothing parameters used in the procedure are chosen as:

- $\gamma = 2$, $\sigma_0 = 10$ and $f = 1.0715$ and
- $\gamma = 2$, $\sigma_0 = 20$ and $f = 1.0715$.

The original surface mesh representing the orthognathic skull shape along with the result obtained from the two registrations are visible in Figure 6.20. Figure 6.20 (a) shows that the three meshes represent the same geometry while the detail of Figure 6.20 (b) shows that there is not a unique representation. The nodal coordinates close to feature registered areas coincide or are closely similar, even when using different smoothing parameters.

The same is done using the prognathic mesh surface as a target in the registration procedure, resulting in three different meshes that represent this shape. The tetrahedral mesh, generated on the average mesh illustrated in Figure 6.16 (b), is

UNIVERSITEIT VAN PRETORIA
UNIVERSITY OF PRETORIA
YUNIBESITHI YA PRETORIA

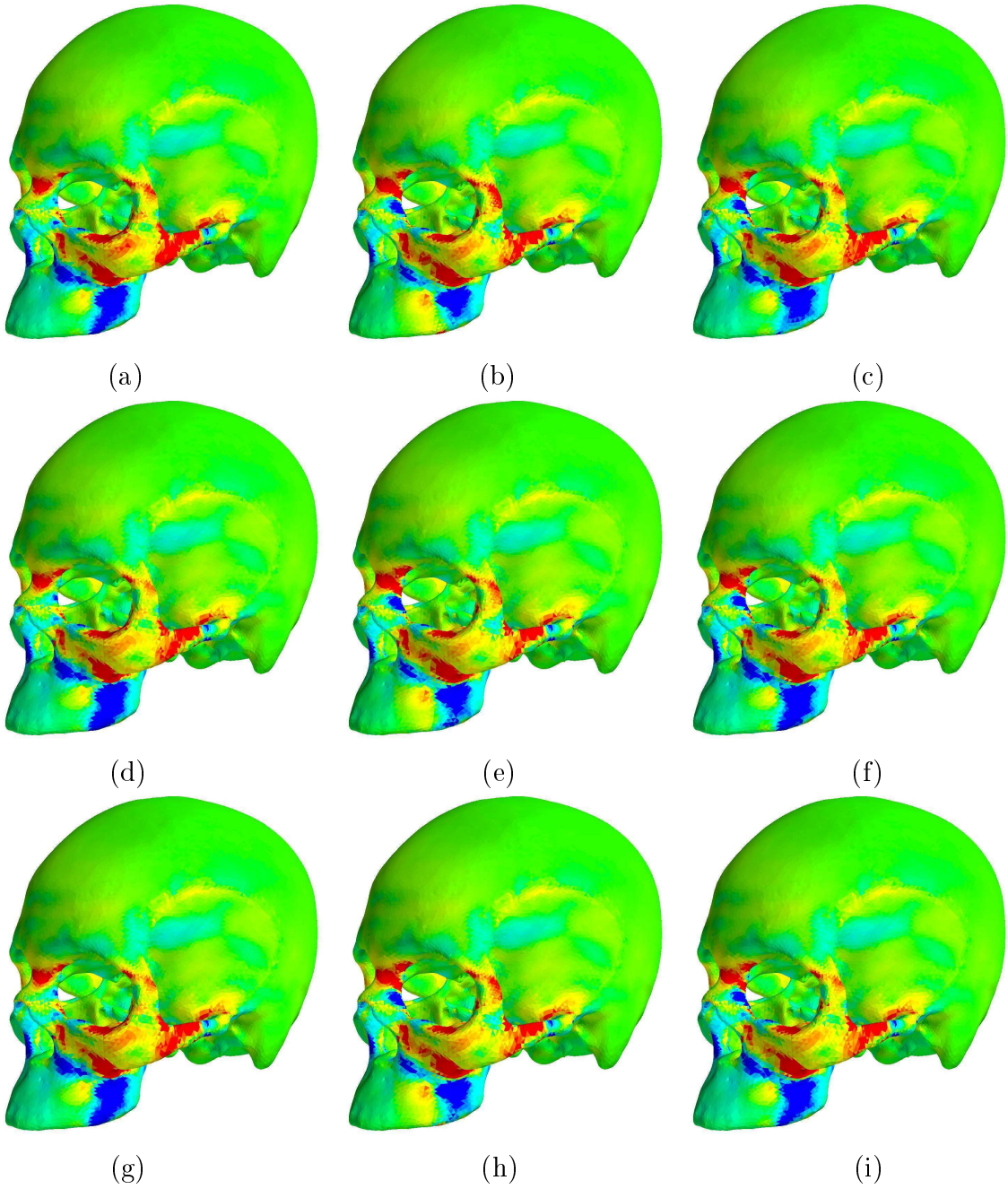

Figure 6.21: The difference in Von Mises stress between the results obtained using different prognathic and orthognathic skull shape mesh representation. Three mesh versions of the prognathic and of the orthognathic skull shape are used. An FEA is done on the molar bite load case using all six meshes. The FEA result on the prognathic meshes is compared to the result on the orthognathic meshes in the same way as Figure 6.19 (c). In each row the same prognathic mesh is compared to a different orthognathic mesh while each column shows the result of the same orthognathic mesh compared to a different prognathic mesh. Contours are given for the range $[-2, 2]$ MPa.

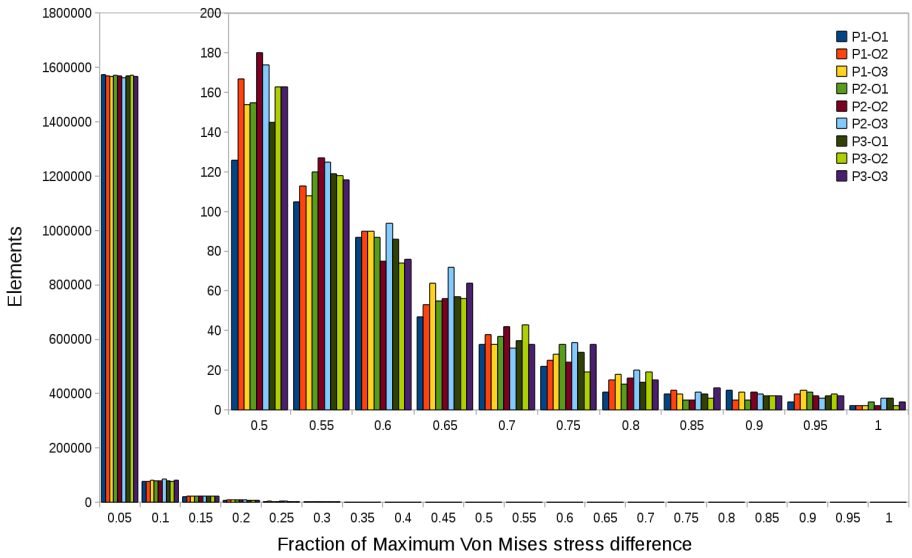

Figure 6.22: Histogram illustrating the distribution of stress variation. The results given in Figure 6.21 is categorised to show the small percentage of elements where a significant variation occur. The absolute value of these results are used and normalised to illustrate them on the same histogram. The majority of elements are seen to fall below 5% of the maximum absolute difference in Von Mises stress.

deformed using the displacement of boundary nodes. This is done as described in section 6.4 and mesh quality improvement is performed to generate usable meshes.

P1 refers to the original prognathic mesh while P2 and P3 refers to the two new prognathic meshes used in this subsection. The three orthognathic meshes are referred to as O1, O2 and O3. The Von Mises stresses of the results on these six meshes are compared in the same way as presented in Figure 6.19. Figure 6.21 shows the difference in Von Mises stress when various combinations of representations are used.

Figure 6.21 (a) is the same results as illustrated in Figure 6.19 (c) but shows contours for $\sigma_{\mathrm{P1}}^{\mathrm{vM}}$-$\sigma_{\mathrm{O1}}^{\mathrm{vM}}$ in the range $[-2, 2]$ MPa. Figures 6.21 (a), (b) and (c) are generated by comparing the same original prognathic mesh result ($\sigma_{\mathrm{P1}}^{\mathrm{vM}}$) with the three different orthognathic mesh results ($\sigma_{\mathrm{O1}}^{\mathrm{vM}}$, $\sigma_{\mathrm{O2}}^{\mathrm{vM}}$ and $\sigma_{\mathrm{O3}}^{\mathrm{vM}}$). The distribution of the absolute difference in Von Mises stress is given in Figure 6.22.

The figures displayed in Figure 6.21 only show contours of the difference in Von Mises stress for the range $[-2, 2]$ MPa with the true range interval for each comparison given in Table 6.2. Slight variation is noted in the difference in Von Mises stress between the prognathic and orthognathic shape when comparing the

	Orthognathic 1	**Orthognathic 2**	**Orthognathic 3**
Prognathic 1	$[-7.978, 12.839]$ MPa	$[-7.171, 12.332]$ MPa	$[-7.584, 12.232]$ MPa
Prognathic 2	$[-8.169, 12.464]$ MPa	$[-7.239, 11.958]$ MPa	$[-7.619, 11.857]$ MPa
Prognathic 3	$[-7.998, 12.367]$ MPa	$[-7.238, 11.860]$ MPa	$[-7.614, 11.760]$ MPa

Table 6.2: Range values for difference in Von Mises Stress. In each case the Von Mises stress result of the analysis of a molar bite on a orthognathic skull representation is subtracted from the same analysis done on a prognathic skull representation per element.

results displayed in Figure 6.21. The greatest deviation is visible for the second column of figures, especially in the bridge of the nose and upper mandible where the bite force is applied. To inspect the variation in the difference in Von Mises stress it is decided to compare the results used to generate Figure 6.21.

In Figure 6.23 the variation in difference in Von Mises stress is inspected. The result obtained when comparing the original prognathic and orthognathic stresses is used as a baseline. Four comparisons are made using the additional two prognathic and two orthognathic meshes along with the original representations. Figure 6.23 (a) is the result used to generate Figure 6.21 (b) $\sigma^{\text{vM}}_{\text{P1}}$-$\sigma^{\text{vM}}_{\text{O2}}$ subtracted from the result used to generate Figure 6.21 (a) $\sigma^{\text{vM}}_{\text{P1}}$-$\sigma^{\text{vM}}_{\text{O1}}$. Contours are displayed for the range $[-0.8, 0.8]$ MPa while the true range for this result is $[-4.93, 5.43]$ MPa. The other three figures also display contours for the range $[-0.8, 0.8]$ and are as follow:

- Figure 6.23 (b) is Figure 6.21 (a) - Figure 6.21 (c). $\left(\sigma^{\text{vM}}_{\text{P1}} - \sigma^{\text{vM}}_{\text{O1}}\right) - \left(\sigma^{\text{vM}}_{\text{P1}} - \sigma^{\text{vM}}_{\text{O3}}\right) = \sigma^{\text{vM}}_{\text{O3}} - \sigma^{\text{vM}}_{\text{O1}}$ has a range of $[-5.20, 5.23]$ MPa.
- Figure 6.23 (c) is Figure 6.21 (a) - Figure 6.21 (d). $\left(\sigma^{\text{vM}}_{\text{P1}} - \sigma^{\text{vM}}_{\text{O1}}\right) - \left(\sigma^{\text{vM}}_{\text{P2}} - \sigma^{\text{vM}}_{\text{O1}}\right) = \sigma^{\text{vM}}_{\text{P1}} - \sigma^{\text{vM}}_{\text{P2}}$ has a range of $[-5.26, 1.99]$ MPa.
- Figure 6.23 (d) is Figure 6.21 (a) - Figure 6.21 (g). $\left(\sigma^{\text{vM}}_{\text{P1}} - \sigma^{\text{vM}}_{\text{O1}}\right) - \left(\sigma^{\text{vM}}_{\text{P3}} - \sigma^{\text{vM}}_{\text{O1}}\right) = \sigma^{\text{vM}}_{\text{P1}} - \sigma^{\text{vM}}_{\text{P3}}$ has a range of $[-2.50, 1.53]$ MPa.

The two additional orthognathic mesh representations have the greatest influence on the variation in difference in Von Mises stress. The average nodal displacement applied to represent each mesh is reported in Table 6.3. Considering the average displacement required from the chosen generic surface mesh to represent this geometry, it makes sense that the registration to the orthognathic surface would be more sensitive to the user specified smoothing parameters. A greater difference

UNIVERSITEIT VAN PRETORIA
UNIVERSITY OF PRETORIA
YUNIBESITHI YA PRETORIA

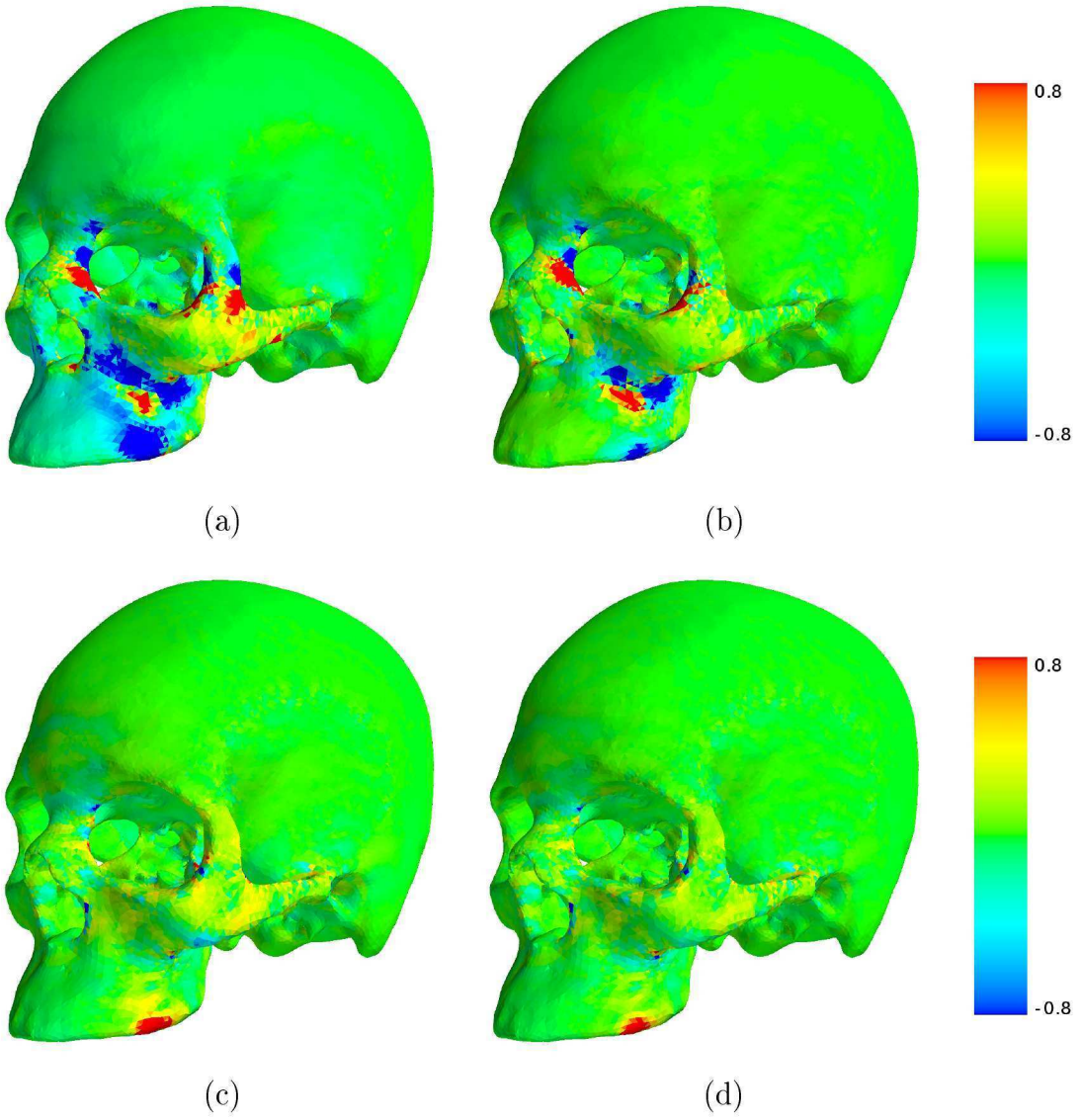

Figure 6.23: The variation of the difference in Von Mises stress using the original results compared to the difference in Von Mises stress when one of the original results is compared with the result on a new mesh representation. (a) Figure 6.21 (a) - Figure 6.21 (b). (b) Figure 6.21 (a) - Figure 6.21 (c). (c) Figure 6.21 (a) - Figure 6.21 (d). (d) Figure 6.21 (a) - Figure 6.21 (g).

UNIVERSITEIT VAN PRETORIA
UNIVERSITY OF PRETORIA
YUNIBESITHI YA PRETORIA

		P1	P2	P3	O1	O2	O3
	Average nodal distances [mm]						
(a)	**surface mesh to base:**	0.583	0.631	0.592	3.557	3.632	3.595
(b)	**tetrahedral mesh to average:**	1.686	1.667	1.671	1.674	1.757	1.720

Table 6.3: Distances from the nodal coordinates on each mesh representation to (a) the position on the generic surface mesh for surface points and (b) the tetrahedral mesh representing the average skull shape.

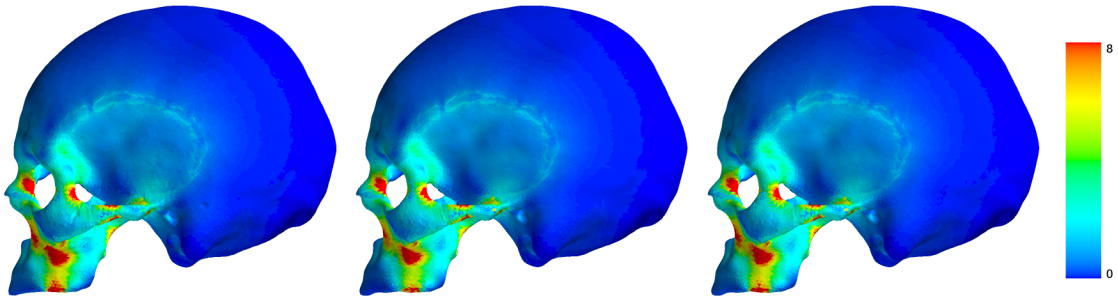

(a) (b) (c)

Figure 6.24: The Von Mises stress result for a molar bite analysis using the same nodes to apply boundary conditions on the three different orthognathic skull shape mesh representations.

in the final nodal coordinates of a mesh representing this shape would be expected due to the greater deformation required.

The Von Mises stress on the three different orthognathic skull representations is visible in Figure 6.24. These results appear to be very similar. The nodes used to apply the boundary condition representing bite force has moved slightly further backward in the second mesh representation of Figure 6.24 (b) when compared to the other two. This would explain the greater variation in the difference in Von Mises stress visible in the upper mandible when this result is compared with the prognathic results.

The elastic registration procedure, uniqueness of the elastic registration result and discretisation of the geometry represented does seem to have an effect on the results of the comparison illustrated in this chapter. If a study on functional morphology or some other comparison on shape and resulting stress field is done using elastic registration or a similar numerical tool, the researcher should use caution when drawing conclusions on the significance of a perceived variation in stress.

Although a slight variation in stress field pattern is visible in Figure 6.21, the

UNIVERSITEIT VAN PRETORIA
UNIVERSITY OF PRETORIA
YUNIBESITHI YA PRETORIA

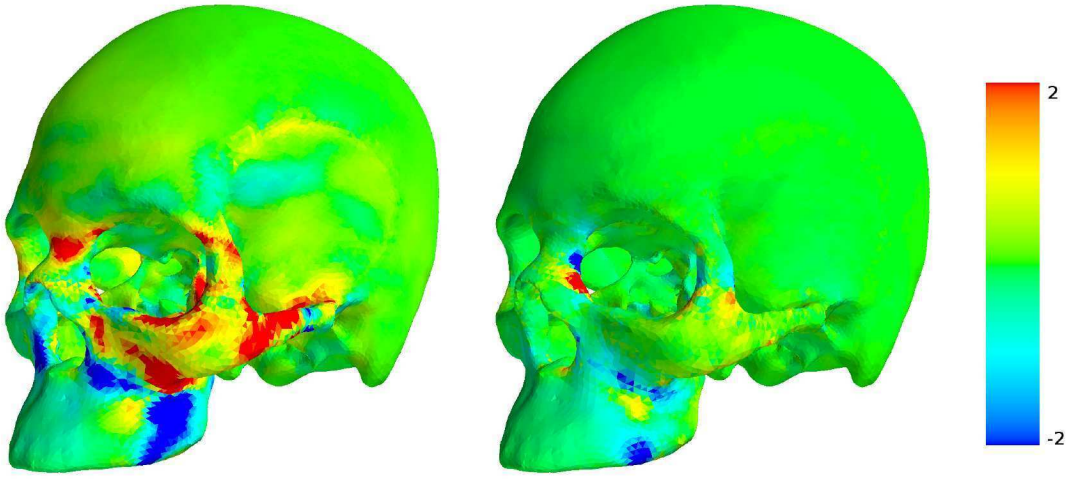

(a) (b)

Figure 6.25: (a) The difference in Von Mises stress for the original prognathic and orthognathic skull analyses also displayed in Figure 6.19 (c). (b) The variation noticed when comparing the Von Mises stress for the original prognathic and second orthognathic skull analyses to the original also displayed in Figure 6.23 (a). Contours are given for the range $[-2, 2]$ MPa.

overall difference in stress field observed here between the two skull forms analysed may likely be attributed to the difference in form and not the uniqueness of the mesh that represents that form. This is communicated in Figure 6.25 where the original comparison is displayed along with the variational result of Figure 6.23 (a) for contours given in the same range of $[-2, 2]$ MPa.

6.5.2 Linearity and constructing an approximate result from principal shape components

The linearity of the problem is illustrated next. The average of the results from an FEA done on the prognathic and orthognathic shape is compared to the FEA done on the average skull mesh. This is done to inspect whether it would be possible to simply construct an approximate representation of the stresses in the average shape from the analyses done on the two ends of the spectrum.

In this example, the average skull is seen as a new skull geometry that requires analysis. The meshes representing the prognathic and orthognathic shapes have already been analysed and it is now desired to check whether it would be possible to approximate the results on the new geometry from the results obtained on the

UNIVERSITEIT VAN PRETORIA
UNIVERSITY OF PRETORIA
YUNIBESITHI YA PRETORIA

meshes representing it's principal shape components.

The results are compared by taking the difference in Von Mises stress. This is because Von Mises stress is rotationally invariant. The difference in stress tensor for instance is not an accurate representation of the actual difference in stress. Stress tensors are recovered from a finite element analysis on different geometries with the same mesh topology. For each different mesh the same element is more than likely to have a different global orientation. A proper interpolation scheme is required or one may compare invariants of the stress tensor such as the eigenvalues (principal stresses).

In Figure 6.26, three different contours are presented on the mesh representing the average skull shape:

- (a) is the Von Mises stress contours for the range $[0, 8]$ MPa resulting from an FEA on the average skull shape with $\max\left(\sigma^{\text{vM}}_{\text{average}}\right) = 15.334$ MPa.
- (b) is the average of the Von Mises stresses for the range $[0, 8]$ MPa resulting from an FEA on the prognathic and orthognathic skull shape with $\max\left(\sigma^{\text{vM}}_{\text{prognathic}} + \sigma^{\text{vM}}_{\text{orthognathic}}\right)/2 = 16.006$ MPa.
- (c) is the difference in Von Mises stress $\sigma^{\text{vM}}_{\text{average}} - \left(\sigma^{\text{vM}}_{\text{prognathic}} + \sigma^{\text{vM}}_{\text{orthognathic}}\right)/2$ for the range $[-0.8, 0.8]$ MPa.

The distribution of the absolute difference in Von Mises stress illustrated in Figure 6.26 (c) is represented in the histogram of Figure 6.27. From this distribution it seems that there is a highly localised area of the skull where significant difference in Von Mises stress is present. The majority of elements vary with less than 5% of the maximum absolute difference in Von Mises stress. This means that the greater majority of elements have an absolute difference in Von Mises stress less than 0.162 MPa with the maximum absolute difference in Von Mises stress 3.247 MPa.

Because the optimisation procedure is required to untangle and improve the quality of the mesh, the coordinates of nodes on the average skull mesh is not the exact same as the average between the prognathic and orthognathic nodal coordinates. The difference between a node on the original average mesh and the location of that node on the average between the prognathic and orthognathic mesh is about 0.181 mm. There are 2402 out of the total of 290569 nodes that differ by more than 0.5 mm and 7 out of those differ by more than 1 mm.

UNIVERSITEIT VAN PRETORIA
UNIVERSITY OF PRETORIA
YUNIBESITHI YA PRETORIA

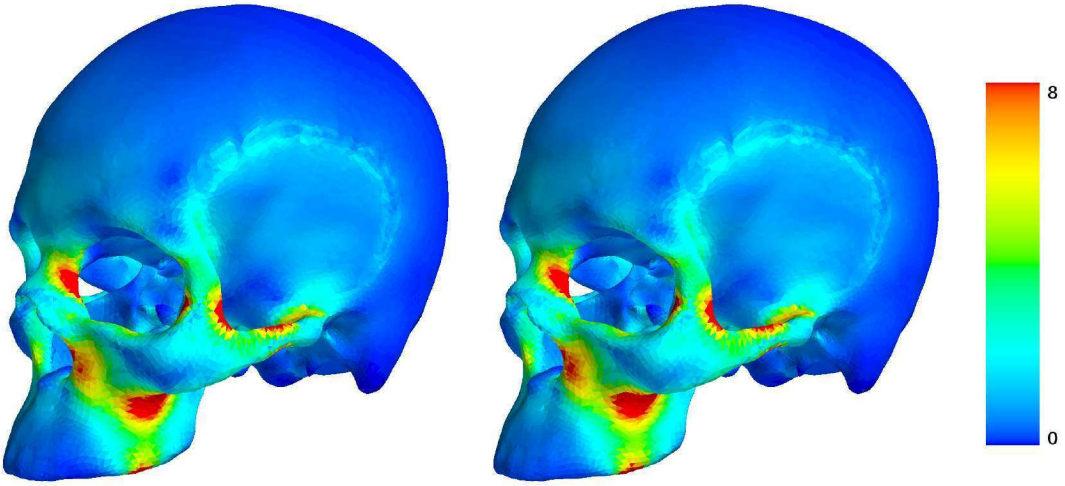

(a) (b)

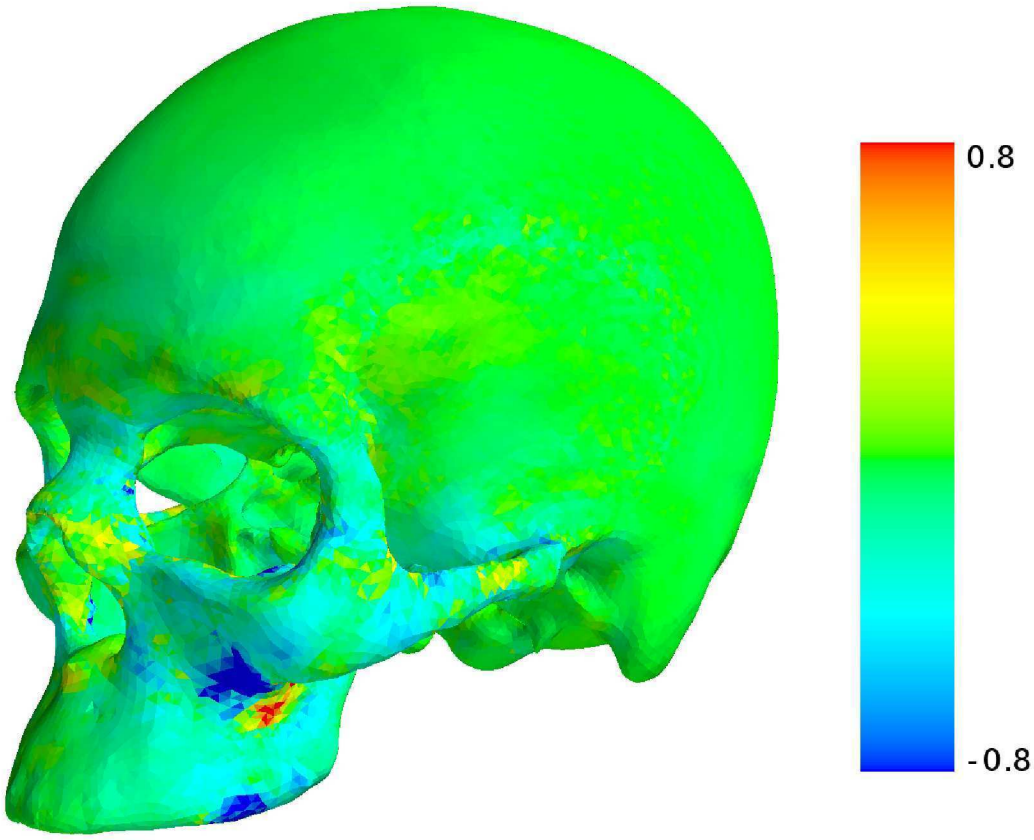

(c)

Figure 6.26: (a) The FEA resulting Von Mises stress on the average skull shape. (b) The average Von Mises result of the prognathic and orthognathic stresses plotted on the average skull mesh. (c) The difference in Von Mises stress $\sigma^{\text{vM}}_{\text{average}} - \left(\sigma^{\text{vM}}_{\text{prognathic}} + \sigma^{\text{vM}}_{\text{orthognathic}}\right)/2$. This falls in the range $[-2.699, 3.247]$ MPa.

UNIVERSITEIT VAN PRETORIA
UNIVERSITY OF PRETORIA
YUNIBESITHI YA PRETORIA

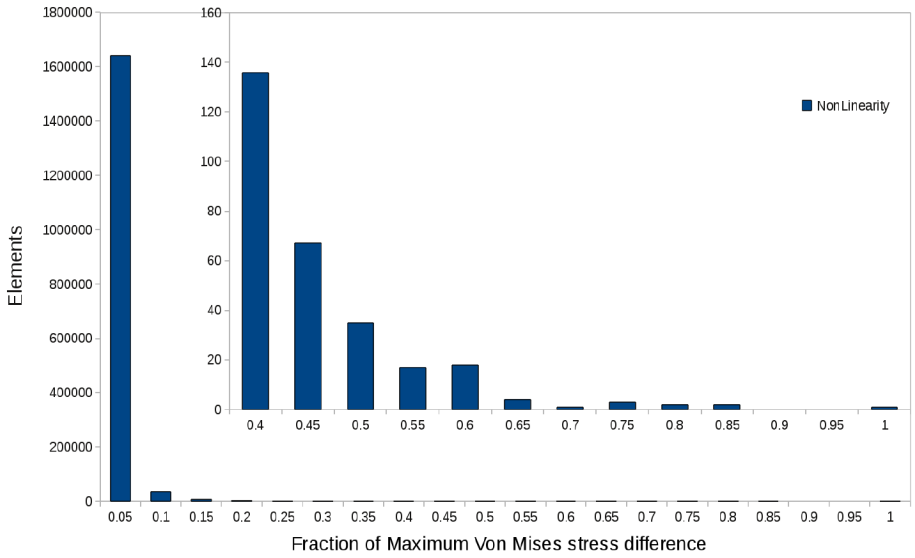

Figure 6.27: Histogram illustrating the distribution of stress variation. The absolute value of the results given in Figure 6.26 (c) is categorised to show the small percentage of elements where a significant variation occur. The majority of elements are seen to fall below 0.162 MPa, which is 5% of the maximum difference in Von Mises stress 3.247 MPa.

As the average mesh used is not exactly the same mesh obtained when taking the average of the prognathic and orthognathic meshes, some of the perceived non-linearity in Figure 6.26 (c) may be due to the non-linearity of the discretisation between these geometries. If one compares the contours that illustrate the sensitivity of discretisation on the compared FEA results visible in Figure 6.23 to this non-linearity of the result in Figure 6.26 (c) for the same range of $[-0.8, 0.8]$ MPa, it seems a very plausible explanation of the perceived non-linearity. Once a fully reliable registration procedure and interpolation scheme is in place, the non-linearity of a specific problem could be quantified or taken into account during comparisons and interpolations between various geometries. A principal component analysis done using a larger statistical sample of geometries may also prove useful in this regard.

If a linear or linearised problem is possible, performing an analysis on a new skull shape wouldn't be necessary. If a new geometry requires analysis, the linear coefficients of the principal modes of variation that approximate this geometry may be obtained. The result on the required geometry may then be approximated using this linear combination of the results on the principal modes.